IMPROVED FLAME FRONT CURVATURE MEASUREMENTS FOR NOISY OH-LIF IMAGES

A.A. Verbeek*, W. Jansen*, G.G.M. Stoffels* and Th.H. van der Meer*

* University of Twente, Laboratory of Thermal Engineering, 7500AE, Enschede, The Netherlands
E-mail : a.a.verbeek@utwente.nl

ABSTRACT

A combination of two common edge detectors is used to obtain a procedure to extract flame fronts from low quality OH-LIF data of premixed flames. The method primarily consists out of a LoG edge detector that uses the Canny edge detector to select the correct edges, based on their overlap. This procedure enables one to extract flame fronts as continuous edges at locations of maximum gradient for low quality OH-LIF data, with SNR as low as 2.7, without the need for user input. The extracted edges can be used to measure, amongst other, flame front curvature. Optimal settings for the parameters involved are determined based on the accuracy and robustness of the method. For this both synthetic and experimental data are used. Although there is some contamination of spurious edges in the set of detected edged (about 1%), the method is able to accurately measure the, for combustion relevant, flame front curvature statistics.

Keywords: *Flame curvature, premixed flames, image analysis, edge detection*

1. INTRODUCTION

An adapted method to measure flame front curvature from OH-LIF images has been developed. By combining two standard edge-detection algorithms a more robust procedure is obtained that is able to successfully process data even with a low signal-to-noise ratio (2.7). An assessment of the accuracy of the measured curvature was made based on synthetic data and the optimal parameters settings are provided for dealing with real experimental data.

Combustion is a widely studied topic, since the majority of energy consumed is produced or converted by combustion systems. The combustion inside these systems is required to produce near zero emissions to keep the environmental impact low. One of the important combustion related pollutant is NO_x, which can cause problems such as adverse respiratory effects, smog and acid rain [10]. Lean premixed combustion [4] has proven to greatly reduce NO_x emissions. In premixed combustion, turbulence is needed to generate wrinkling and corrugation of the flame and thereby increasing the overall combustion rate in burners [9]. Here, the question arises of what specific turbulence is most effective for this purpose and how this should be introduced into a flow. In [16] an attempt is made to enhance combustion of a burner by introducing specific turbulent modes in the upstream flow. In order to experimentally investigate the effect of turbulence on the wrinkling of the flame front, OH-Laser Induced Fluorescence (OH-LIF) is often applied. A subsequent processing algorithm is usually needed to extract the curvature of the flame front from the 2D OH-LIF images.

There are already methods described to measure flame front curvature from OH-LIF [3, 6, 12, 14, 18], but there is a need for a robust method that is able to processes low-quality OH-LIF data with predefined settings. Usually a particularly setting won't work for all frames, due to noise and intensity changes. Furthermore, no user-intervention is desired. In, for example, [3] edges are manually compared with the original OH-LIF data to judge the validity of the retrieved edge. When analyzing extensive data sets and investigating a large parameter space this can be very cumbersome.

In this work a new approach is presented in which edge detection is performed by a combination of two common
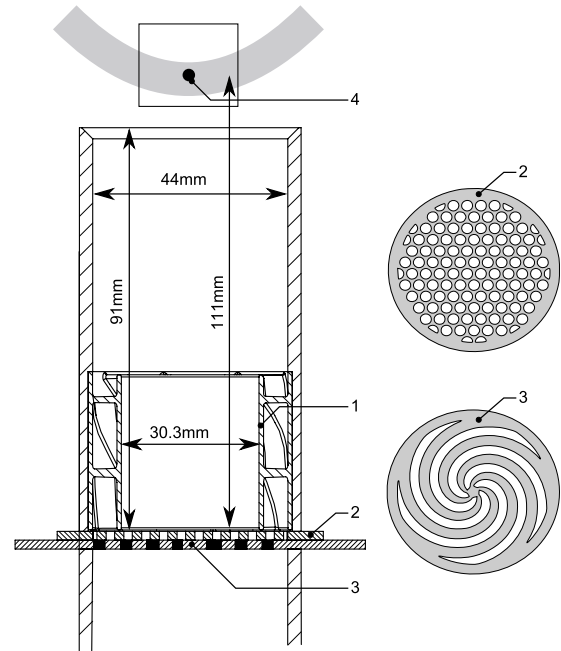

Figure 1: Schematic view of the used low swirl burner with active grid. (1) swirler, (2) static disk, (3) rotating disk, (4) approximate location of the flame

edge detection algorithms (Canny and LoG). Optimal parameter settings are determined for our low quality data and the robustness of the method is investigated by comparing its performance against human interpretation. Furthermore, the effect of the errors made by the method on the measured curvature is quantified. This show that results can be directly used and no further used intervention is needed.

The organization of the paper is as follows. The experimental setup is discussed in section 2.1. This will briefly explain the burner and describes the equipment used for obtaining the OH-LIF images. Section 2.2 will provide a full description of the edge detection algorithm. In section 3 the performance of the method is tested and quantified. Concluding remarks are made in section 4.

2. EXPERIMENT

2.1 How is the OH-LIF data acquired?

The OH-LIF images that are used in this work are obtained from a low swirl burner [2] in combination with an active grid as described in more detail by Verbeek et al. [16]. In fig.1a schematic of the used burner is depicted. Due to the absence of a recirculation zone in Low-Swirl burners, the central part of the flame is only wrinkled by the upstream applied turbulence. Therefore, this burner is particularly suited for investigating the interaction of turbulence and combustion. The burner consists of a tube with an inner diameter of 44 mm and a length of 91 mm. Swirl is added to the flow in the outer annulus by a swirler. The central part of the flow remains axial, but turbulence is added by active grid composed of a rotating and a static perforated disk. At approximately 20mm downstream of the burner exit the flame will stabilize. The region from where the flame front is captured is indicated by the rectangle in fig.1.

OH-LIF is a common technique to capture the instantaneous geometry of premixed flames [5]. An example of an image obtained by OH-LIF is shown in fig.3a. Laser light of a well-defined wavelength is used to electronically excite specific, combustion related, molecules. Upon relaxation of the molecule fluorescence is emitted which is captured by an intensified camera. The combustion related species can be, for example, OH, CH or NO. For visualizing the premixed flame front, OH is the species of choice. OH is formed at the flame front and remains present in the burned gasses, which makes it relatively simple to discriminate between burned and unburned regions and to locate the interface, i.e., the flame front. An alternative would be CH-LIF. Since CH is only present at the reaction zone itself, it will directly provide the location of the flame front. However, the significantly lower intensity of the fluorescence makes this method less favorable. Identifying the burned and unburned regions based on the CH-LIF data will be complicated for heavily corrugated flame fronts.

2.1.1 Equipment

To obtain 2D cross sections of the flame by OH-LIF a tunable laser, sheet forming optics and a intensified camera are used. An excimer pumped dye laser (Lambda Physik LPX 240i in combination with Lambda Physik Scanmate 2, Coumarin-153 Dye dissolved in Methanol) is used to generate light with a wavelength near 283 nm. The laser is tuned to the $P_1(2)$ line @282.56 nm of the $A^2\Sigma^+(v'=1) \leftarrow X^2\Pi(v''=0)$ absorption band, since this resulted in the strongest fluorescence signal. The pulse energy is about 0.3 mJ.

The laser beam is converted into a planar sheet by using five lenses as indicated in fig.2. The first two, forming a telescope, are used to decrease the size of the incoming beam. The subsequent two cylindrical lenses convert the beam into a sheet with a height of approximately 25 mm. To obtain true 2D cross sections of the flame a sufficiently thin sheet is needed. By using an additional transversely cylindrical lens the thickness of the sheet is kept below 150 μm. This value is smaller than the typical flame front thickness of 0.5 mm and also smaller than the expected size of the wrinkles in the flame front (in the order of 0.4 mm based on similar experiments of [3, 6]) and the sheet should therefore be sufficiently thin.

.

The fluorescence is captured with an image intensifier (LaVision HS-IRO) together with a CCD camera (Redlake
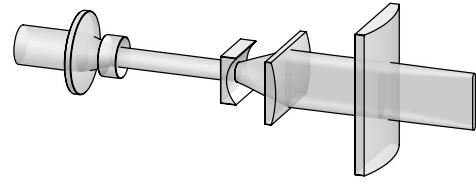

Figure 2: Sheet forming optics.

MotionScope 1000S). As objective the Cerco UV lens 45 F/1.8 is used. Since the minimum focus distance of 60 cm results in insufficient resolution an additional convex lens (f=100 mm) is placed in front of the objective to provide for additional magnification. The complete configuration captures a region of the flame of 18.0×15.7 mm with a resolution of 480×420 px (37.5 μm/px).

A data set of 915 frames that was recorded with the described setup is used in this work to analyze the performance of the new edge detection method.

2.1.2 Quality of the data

As a measure of the quality of the OH-LIF data, the signal to noise (SNR_{LIF}) is used. It is defined by eq.1 [13], where μ and s stand for the mean and standard deviation of the signal. The subscript b and u indicate the burned and unburned state respectively. To extract the intensity data unambiguously from the burned and unburned areas the edge region itself is disregarded, i.e., the data points less than 10 px away from an edge are excluded. Only regions of similar size are compared, which means that only frames with a fraction of burned area between 30 and 70% are used. The SNR_{LIF} for the data set that is used for this study varies between 1.4 and 5.5 with a mean of 2.7 and can be considered as low compared to [13, 15].

$$SNR_{LIF} = \frac{\mu_b - \mu_u}{s_b} \qquad (1)$$

2.2 Edge detection

Many different edge detection algorithms where tested for their ability to flawlessly detect the flame fronts present in the image. In fig.3a an example is shown of a captured image. Although this task seems to be trivial for human perception, implementing these computationally proved to be a challenge.

The simplest method would be converting an image to a binary image based on an intensity based threshold. However, this results in poor localization of edges, since the user has to set an appropriate threshold value. Although standard methods are available for this selection [8], the detected edge usually does not correspond with the location of the highest gradient. As an example in the top of fig.3a there is a small decrease in signal, where at some location the threshold will be crossed. A detected edge at this location is clearly not a physical one.

The step to a gradient based method is easily made when edges are to be found at locations of maximal gradient. One method that results in good localization of edges is the Laplacian of Gaussian (LoG) method described by [7]. This provides edges at zero-crossings of the Laplacian, ∇^2, of the Gaussian smoothed

image. (This marks the location of maximum gradients) Besides good localization it provides continuous edges. The drawback is that a threshold is needed to separate between physical edges, having high gradient, and non-physical edges found in regions of a more uniform intensity (see fig.3b-c).

A popular, more advanced edge detection method is the Canny method [1]. It uses a more elaborate algorithm, which also uses the image gradient, but it differs by incorporating linking of several edge fragments and hysteresis in the threshold value. Although the method is most robust in our perspective from all standard methods, it is not suitable for curvature measurements, since especially at the linking of several fragments unnatural curvatures are introduced. Furthermore, a tradeoff must be made between the number of physical edges found in a continuous manner and the number of spurious edges. This is illustrated in fig.3d-g.

2.2.1 Combination of LoG and Canny

To improve the success-rate of the edge detection, the two latter standard methods are combined. We use the edges detected as the zero-crossings of the LoG-filter, which are always closed contours or connected to the border of the image, but we select only those that overlap with the edges found by the Canny algorithm. The reason that continuous edges are preferred or rather required is that continuous edges make it possible to binarize the image in burned (1) and unburned (0) regions. Without closed edges this would be ambiguous.

Fig.3h shows the example frame with both the LoG and Canny edges. The edges considered as 'physical' are not found at exactly the same location by the two separate methods. Therefore, the number of overlapping pixels for each LoG edge, N_O^i, is calculated by the number of pixels from a thickened or 'dilated' LoG edge, $N_{L,D}^i$, overlapping with the pixels of Canny edges, N_C. The overlapping ratio, O_i is than defined by the ratio of N_O^i and the number of pixels from the LoG edge, N_L^i, see eq.2.

$$O_i = \frac{N_O^i}{N_L^i} = \frac{N_{L,D}^i \cup N_C}{N_L^i} \qquad (2)$$

2.2.2 Output of edge detection

Once the edges are detected additional processing is needed to obtain flame front curvatures, but also for evaluating the progress variable (burned/unburned) or flame surface density.

To be able to calculate the curvature, as defined by eq.3, along an edge composed of discrete pixels, first a continuous description is needed. This is done by fitting a smoothing spline [11] through the edge pixels. Such a spline is allowed to deviate somewhat edge pixels, but creating thereby a differentiable parameterization of the edge. The maximal deviation allowed is controlled by a new parameter, the spline tolerance, f, which is the maximal allowable distance between the edge pixel and the spline. The sign of the curvature is defined positive when the center of curvature is positioned in the unburned zone. By checking the sign of the image intensity derivative in the normal direction at a single location in the flame front it is determined if this is the case. If not the sign of curvature is flipped for the corresponding edge.

$$\kappa = \frac{x'y'' - y'x''}{\left(x'^2 + y'^2\right)^{3/2}} \qquad (3)$$

The progress variable (PV) each region, i.e., 1 for burned or 0 for unburned, is determined by comparing the mean intensity of the largest region with the Otsu threshold [8] of the total image. Although this method was considered as inadequate for edge detection, for determining the state of the regions it provides a robust threshold value without requiring user input. With the PV known in a single region, the PV for the remainder of the frame is evident. It is alternating for every adjacent region.

2.2.3 Methods parameters

The newly proposed method consist of several parameters that need to be set a-priori. Each of these parameters will be addressed in how it affects either the robustness of the edge detection or the accuracy of the detected curvature. The parameters are to be divided in these two groups as displayed in table 1. In the next section appropriate values for these parameters will be deduced and presented. Besides these five parameters there are a few other parameters, which will not be discussed further, either because the value was set according to literature or it is of little influence. However, for completeness they are summed here.

1. The lower threshold in the Canny's edge detector, t_{CL}, is set to $0.4t_{CH}$ as implemented in the edge MATLAB-routine and also suggested by [1].

2. The size of the Gaussian smoothing mask, m_σ, is set to $6\sigma \times 6\sigma$. With such a mask-width the integral of the 2D Gaussian function is within 1% deviation of the same integral on an infinite sized mask. It is also the default value of edge MATLAB-routine. Increasing m_σ did not reveal an improved accuracy in the detected curvature, while computational power significantly increased.

3. To obtain the smoothed image in the region closer than $0.5m_\sigma$ to the border, information from outside the domain is needed. Although the default MATLAB implementation uses here the value of the nearest border pixel, there is no physical justification to do so. After determining the edges with both methods the result is cropped $0.5m_\sigma$ from the frame border.

4. The continuous representation of the spline is realized with a cubic smoothing spline, which can be obtained by invoking the spaps MATLAB-routine. A cubic spline fulfills the requirement of being twice differentiable which is needed to calculate the terms in eq.3.

5. For very short edges it is not possible to obtain a cubic spline representation. Therefore edges smaller than 20 px in length are discarded.

Table 1: Parameters involved in the new edge detection method. The first two affect the accuracy of the detected curvature, while the latter three will influence the robustness of the edge detection process.

| Symbol	Description	Unit
σ	Standard deviation of the Gaussian smoothing. Used for both LoG and Canny edge detector	[px]
f	Maximum allowable distance between edge pixels and smoothing spline.	[px]
t_{CH}	Upper threshold of the Canny edge detector.	[-]
t_O	Threshold value for minimum overlap ratio of LoG and Canny edges.	[-]
d	Thickening of the LoG edge before comparing it with the Canny edges.	[px]
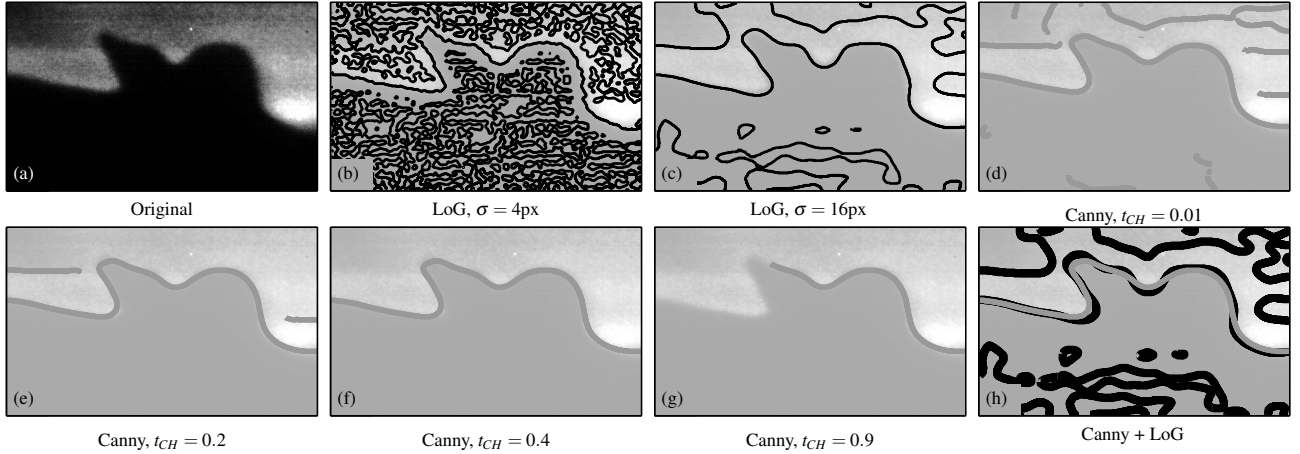
Figure 3: From top left to bottom right: (a) Original OH-LIF image. (b,c) All edges found by the LoG method for σ=4 and 16 (d-g) Edges found by Canny method for different threshold values, t_{CH}=0.01, 0.2, 0.4 and 0.9, with σ=16. The value of t_{CL} is kept fixed relative to t_{CH}, i.e., t_{CL}=0.4t_{CH} (h) Combination of Canny and LoG method.

3. RESULTS AND DISCUSSION

What are the optimal settings for the new edge detection method when applying it to data obtained with the experimental setup as described in 2.1? In this section an answer will be given to that question. In 3.1 synthetic data is being subjected to the edge detector to investigate how the accuracy of the measured curvature is affected by σ and f. In 3.2 the effect of t_{CH}, d and t_O on the robustness of the edge-detector is examined when applying it to real experimental data. In 3.3 the overlap based thresholding of the new edge detection method is compared to a more conventional thresholding. Finally, in 3.4 the statistics of the flame front curvature that follow from the method are compared with those that follow from human interpretation.

3.1 Accuracy

Some smoothing is necessary in the edge-detection process to suppress the influence of noise, but this also eliminates small scale details present in the flame front. Also the smoothing spline that is used to obtain a continuous description of the retrieved edge has an influence on the accuracy of which small scale details can be resolved. The extend of this behavior is quantified by applying the method to synthetic data with known curvatures. The synthetic data used consists of circles with radii ranging from 1 to 120 px. To obtain different rasterized representations of the same circle, the circles are generated on a six times larger grid where there origin is shifted between 0 and 5 pixels in both horizontal and vertical direction. Upon downsampling the multiple rasterizations are realized. The advantage of using circular data is that curvature along the boundary is constant such that methods ideally returns a Dirac delta function shaped distribution for the measured curvature.

3.1.1 Effect of σ

The effect of varying σ is shown in fig.4. Here the mean value of the measured curvature ($\bar{\kappa}$) is normalized by the analytical curvature (r^{-1}) and plotted against the circle's radius
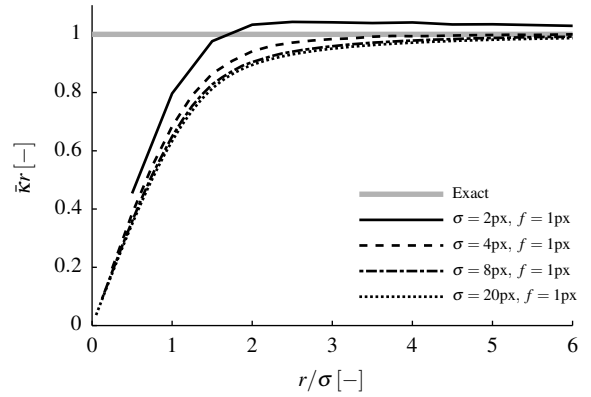

Figure 4: Normalized graph of the measured curvature as function of the circle radius for different values of σ.

(r) normalized by σ. This normalizations makes the graphs for different σ more or less collapse.

It can be seen that the edge detector acts as a low-pass-filter. When features are small, i.e., small compared to σ, the curvature is seriously underestimated. As a rule-of-thumb for the user it can be stated that curvatures can be measured with an error within 10%, when $r/\sigma \geq 2$.

Although one can state that the lines more or less collapse, there is some difference. Using a smaller σ results in higher measured curvature, with for $\sigma = 2$ a measured curvature even higher than the analytical value. This can be explained by the behavior of the smoothing spline, that is allowed to deviate f px from detected edge, resulting in a circular spline with a radius f px smaller than the radius of the detected circular edge. For small σ this effect is more prominent and can even lead to over prediction of the curvature. However, the error less than 10% is still guaranteed for $r/\sigma \geq 2$.

3.1.2 Spline tolerance

Variation of f is also studied. In fig.5b the signal-to-noise ratio (SNR) of the curvature is plotted as function of the circle radius. This SNR is defined by the mean curvature divided by the standard
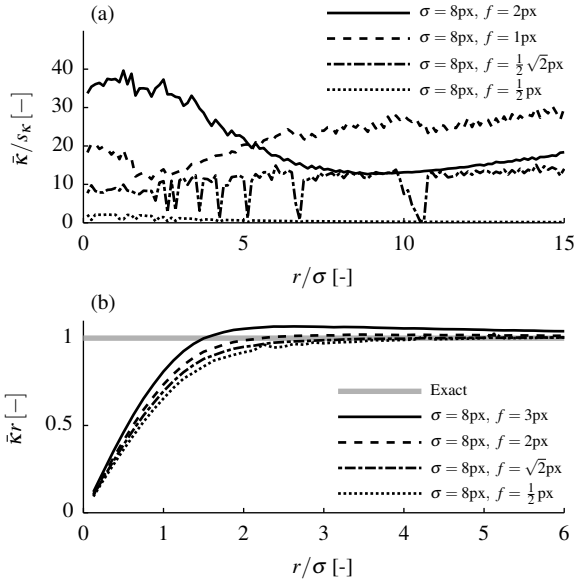
Figure 5: (a) Signal-to-Noise ratio of the measured curvature as function of r/σ. (b) Normalized graph of the measured curvature as function of the circle radius for different values of f.
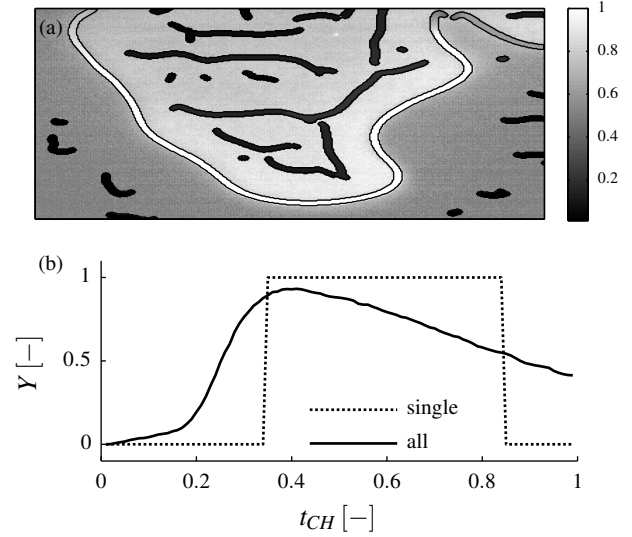
Figure 6: (a) LIF image with on top the Canny edges colored by the maximum value of t_{CH} upon which the location is included as edge. The gray scale applies only to the edges and not to the background. (b) The dotted line indicates the window for t_{CH} for succesfull detection of physical edges by the Canny filter for the specific frame. The solid line represents the window averaged over all frames.

deviation of the curvature. Using a tolerance below $\frac{1}{2}\sqrt{2}$ px gives very poor results, since the SNR is in the order of 1. Using exactly $f = \frac{1}{2}\sqrt{2}$ px occasionally results in a low SNR, but using a value of 1 px or higher provides satisfactory results, with an SNR larger than 10 for all radii. Due to the discrete steps made by the edge pixels, which are round-off effects, the spline curve needs to 'cut off the corners' somewhat to give a smooth representation of the edge. To represent a straight line which is not exactly horizontal or vertical, the pixels deviate up to $\frac{1}{2}\sqrt{2}$ px from the line and therefore a spline reconstructing the original line should at least have a tolerance $\frac{1}{2}\sqrt{2}$ px. This minimum value is also supported by the results of the processed synthetic data with different f.

Using a spline tolerance introduces an offset in the obtained curvature as could already be seen from fig.4. In fig.5a again $\bar{\kappa}r$ is plotted as function of r/σ, but since solely f is varied for the different lines, this illustrates very well the effect of f. The spline cuts off at edges with high curvatures due to its nature of its definition. For a circle with radius r this means that the corresponding spline describes a circle with radius $r - f$. This corresponds with the fact that a higher curvature is detected when f is larger.

To control the error in curvature of this effect, f should be much smaller than the radii present in the image. Increasing the tolerance much above the minimum value of $\frac{1}{2}\sqrt{2}$ px does not increase the accuracy further, so it is recommended to set f to 1.

3.2 Experimental data.

While the previous subsection discussed the accuracy of which the LoG edge detector together with the smoothing spline is capable of resolving curvatures present in the data, in this subsection the performance of the complete algorithm is assessed. This is done by analyzing how well the algorithm selects only physical edges from the clutter of edges that the LoG edge detector retrieves from our OH-LIF data.

3.2.1 Canny threshold

In order to obtain the optimal value for t_{CH}, the performance of solely the Canny edge detector is evaluated for our dataset. First, for every frame of the dataset a window is determined for t_{CH} in which the result contains only physical edges. Secondly, the averaged window for all frames is determined of which the maximum is used to obtain the optimal value for t_{CH}. At this value the most physical edges are included.

To obtain the window for a certain frame I, the outcome of the Canny edge detector, $X = \text{canny}(I, t_{CH})$, is averaged for t_{CH} between 0 and 1, i.e., $\bar{X} = \int_0^1 \text{canny}(I, t_{CH}) \, dt_{CH}$. Since X contains either ones for edge pixels and zeros for all other pixels, in the averaged result, $\bar{X}$, every edge pixel is evaluated between 0 and 1 indicating up to which threshold value this pixel will be evaluated as being part of an edge. This result is displayed in fig.6a. By manually selecting the physical edges from $\bar{X}$, the window for t_{CH} for the specific frame is determined, see fig.6b. At the lower end of the threshold window all unphysical edges are only just suppressed, while at the upper end the less pronounced physical edge is about the be suppressed. The averaged window is also plotted in fig.6b.

Since the Canny edge detector can create discontinuous edges, with the endpoints usually already excluded from the result for low values of t_{CH}, some attention is needed here. In fig.6a the endpoints of the two major edges are clearly of different value than the main part of those edged. By including only the 90% highest valued pixels of an edge marked as physical, the ambiguous regions are automatically omitted.

From the averaged window of fig.6b it follows that optimal value of t_{CH} is about 0.41. To be on the save side, so further away from the steep descent where a lot of incorrect edges will be included the value of 0.45 will be used.

3.2.2 Overlap of Canny and LoG

With the overlapping of the Canny and LoG edges as the basis

of the newly proposed edge detector, here the parameters involved specifically in this overlap are analyzed. These are the amount of dilation of the LoG edge d and overlapping ratio threshold t_O.

To objectively determine optimal values for both t_o and d the χ^2-metric is used similar to [13, 17]. In this analysis the outcome of the selection of LoG by the algorithm is compared to the ground truth (GT), which is the outcome of manually selecting physical LoG edges. For every evaluated LoG edge there are four possibilities, as summarized in table 2. χ^2 is defined by eq.4 and is maximized as $\chi^2 = 1$, when the outcome of the algorithm is identical to the GT.

$$\chi^2 = \frac{\frac{TP}{TP+FN} - TP - FP}{1 - TP - FP} \cdot \frac{TP + FP - \frac{FP}{1-TP-FN}}{TP + FP} \quad (4)$$

All LoG edges are detected from the 915 frames of the dataset for σ=10, 12 and 16. For every edge it is determined if the edge is either physical or not. When part of an edge is unphysical, the complete edge was rejected.

Dilation of LoG edges

In fig.7 the maximum χ^2 value is plotted as function of d/σ for the different values of σ. It can be seen that using a higher d results in a higher χ^2 for all σ. However, using a d higher than $\frac{1}{2}\sigma$ doesn't significantly increases χ^2. It is therefore suggested to use $d = \frac{1}{2}\sigma$. The difference in localization of the Canny and LoG edge detectors is expected to scale with σ and this also suggest an asymptotic trend in overlap between Canny and dilated LoG edge for increasing d. Physical edges will have more overlap with the Canny edges for higher d, which makes it easier to separate them from the non-physical ones. This behavior is expressed in a higher χ^2 as observed.

Overlap threshold

The effect of variation of the minimum overlap ratio threshold, t_O is shown in fig.8. For different values of σ, χ^2 is calculated as function of t_O. For the dilation $d = \frac{1}{2}\sigma$ was used. What immediately becomes clear is that there exists a large plateau where χ^2 is barely effected. This plateau of high χ^2 extends at least up to $t_O = 0.5$, meaning that for this parameter range the method performs fairly constant and making the choice for t_o not critical.

It can be seen that the algorithm performs better for $\sigma = 16$ than for the lower two values, based on the higher χ^2. This can be understood by the fact that a higher σ results in more suppression of noise, making edge detection more successful for both Canny and LoG.

Table 2: Edge selection outcome possibilities

| Symbol	Definition
TP	True Positive (hit). Fraction of edges classified as good in GT and by algorithm.
TN	True Negative (correct rejection). Fraction of edges classified as bad in GT and by algorithm.
FP	False Positive (false alarm). Fraction of edges classified as bad in GT, but as good by algorithm.
FN	False negative (miss). Fraction of edges classified as good in GT, but as bad by algorithm.
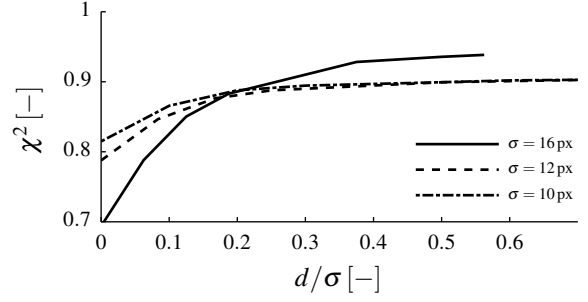
Figure 7: χ^2 as function of amount of dilation, d, of the LoG edge before calculating the overlap ratio for different σ.
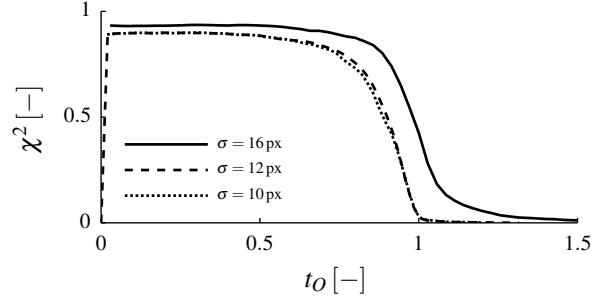

Figure 8: χ^2 as function of minimum overlap value, t_O, at which a LoG edge is included as a good edge.

3.3 Comparison with gradient thresholding

From the previous subsection is follows that there exist a parameter settings range for which the presented edge detection method works optimal for our low quality OH-LIF data. Within this range the performance of the method is not much effect, making it a robust method. In this subsection the performance of the new method, which is basically a LoG edge selector, is compared to a more conventional selection method.

A usual implementation of a LoG edge detector involves a threshold based on the strength of the zerocrossings of the LoG of a data image, to select which pixels are marked as an edge. Using any threshold value higher than zero will result in broken edges, making such method unfavorable for our purpose. As an alternative the averaged strength of the zerocrossing for the complete edge can be used as a selection criterion. This strength is computed by averaging the gradient of the LoG of an data frame over the edge pixels of a given LoG edge, i.e. $\overline{\nabla LoG}$. A threshold value, $t_{\overline{\nabla LoG}}$, is then used as a minimum for $\overline{\nabla LoG}$ for the LoG edge to be marked as a good one.

Fig.9 shows the comparison between the two different edge selection methods. In fig.9a-b histograms of the selection criterion value for the physical and non-physical edges are shown. Already from these graphs it becomes clear that by using the overlap ratio as criterion, a better separation between the physical and non-physical edges is obtained. The distributions as function of $\overline{\nabla LoG}$ show overlap in a large range.

When looking at TP and FP (fig.9c-d), i.e., the data that will be used to obtain statistics about the flame geometry, as a function of the threshold value the same difference in separability is visible. The rate of false edges (FP) is about two orders of magnitude lower than the rate of true edges (TP) over a broad range of t_O, while for $t_{\overline{\nabla LoG}}$ such a stable range cannot be identified. However,

there is a narrow range of $t_{\overline{\nabla LoG}}$ where non-physical edges are well suppressed, while preserving physical ones. This is most clearly expressed in the χ^2-metric, as plotted fig.9e. The maximum value for the gradient based thresholding is slightly higher than of the overlap based thresholding, but only in a narrow range. This makes the $\overline{\nabla LoG}$-based method less robust, since the optimal value of $t_{\overline{\nabla LoG}}$ will depends on the absolute intensity and quality of the data. Selection based on overlap ratio will not suffer from this deficiency and is therefore favorable.

It should be noted that for both method it is not possible to obtain a high ratio of TP/FP without rejecting some of the physical edges. There are edges marked as physical in the GT that show no overlap with Canny edges or have a low value of $\overline{\nabla LoG}$. A low SNR of the OH-LIF data make inevitable that some physical edges will not be detected. However, by using a threshold value of $t_O = 0.5$, 1163 out of the 1293 physical edges are included in the result with a contamination of only 12 non-physical edges (for $\sigma = 12$). Frames with low quality data are expected to contain the same statistical information about the flame geometry, since the low quality is either caused by a low pulse energy or jitter in the timing of the equipment, instead of changes in the flame itself. Rejecting some low quality data is therefore not disadvantageous.

With only 1% of erroneous data, information like the mean progress variable or the flame surface density can be accurately determined. It is also considered acceptable to obtain flame front curvature distributions as will be discussed in the next subsection.

3.4 Flame front curvature

By using the overlap ratio to select good edges from the set of edges obtained by the LoG edge detector inevitably some incorrect edges will be included in the result. To see to what extend this influences the statistical properties of the flame front curvature, the curvature distribution (PDF) of different sets of edges are shown in fig.10.

The PDF of the sets with $O > 0$ and $O > 0.5$ show an excellent agreement with the PDF of the GT when plotted on linear scale, see fig.10a. In order to indicate the difference between the curvature of physical and non-physical LoG edges also the PDF of the complete set is depicted, which shows no resemblance with the GT. As long as the edges with no overlap are excluded, the PDF has the proper shape. However, when plotting the PDF on logarithmic scale the benefit of using a threshold value, $t_O = 0.5$, becomes clear. The PDF for $O > 0$ start to deviate from the GT for $\kappa < -3\text{mm}^{-1}$ and $\kappa > 3\text{mm}^{-1}$, while when using $t_O = 0.5$ the PDF is almost exactly the same as the PDF of the GT.

Statistical moments like the standard deviation and the skewness are determined for the three distributions and plotted in fig.10c-d. The data set with all edges is left out of consideration here. Also these figures indicate that by using a threshold value $t_O = 0.5$, the statistical properties of the GT are well approximated. For higher statistical moments more deviation between GT and $O > 0.5$ is observed, but since these quantities are more and more dominated by a low number of extreme values, they are not relevant for studying combustion. More relevant is at what curvatures the majority of the flame front resides.

Although some data that is present in the GT, but not in the set with $O > 0.5$, the same basic statistics are observed for both sets. This means that the missing data (FN) does not contain different statistical properties than the data that is included in the result. Missing 10% of the data, like in the analyzed case, is not a disadvantage, as previously assumed. The contamination of false edges is limited, i.e., in the order of 1%, and does not complicate
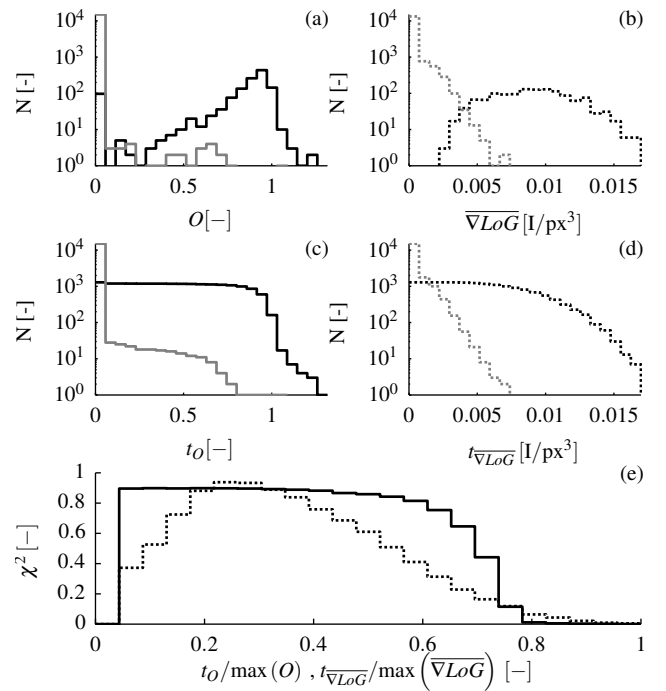

Figure 9: (a) Histogram of overlap ratio for all physical LoG edges (black) and non-phsical LoG edges (gray). (b) Histogram of the mean gradient value of the LoG at physical edges (black) and non-physical edges (gray). (c) TP (black) and FP (gray) as of the overlap threshold value, t_O. (d) TP (black) and FP (gray) as function of threshold based on gradient of the LoG, $t_{\overline{\nabla LoG}}$. (e). χ^2-metric for threshold based on overlap with Canny edges (solid) and based on the mean gradient of LoG (dotted). The data of all the subfigures correspond to $t_{CH} = 0.45$, $\sigma = 12$ px and $d = \frac{1}{2}\sigma$.
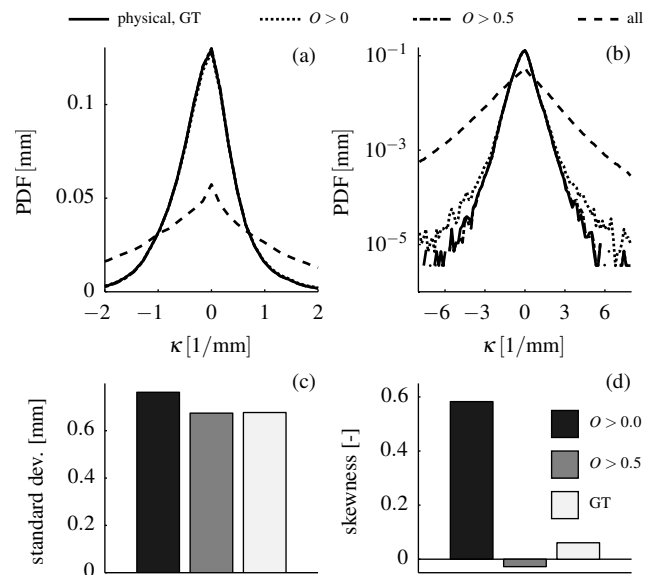

Figure 10: PDF of curvatures of different sets LoG edges plotted on a linear (a) and logarithmic (b) vertical axis. (c) Standard deviation of PDFs. (d) Skewness of PDFs.

to obtain statistics of the flame front geometry that are relevant for combustion.

4. CONCLUSIONS

A robust method to detect flame fronts in OH-LIF images was presented. By combining two different standard edge detection methods (the LoG method and the Canny method) an algorithm is obtained to measure flame front curvatures accurately, without the need for additional user intervention. The method primarily consists out of a LoG edge detector, which uses the Canny edge detector to select correct edges, based on their overlap.

To acquire the optimal parameter settings, five parameters were varied: σ, f, t_{CH}, t_O and d. For t_{CH}, t_O and d the values were chosen such that the highest success-rate in detecting flame fronts as edges was obtained, i.e., $t_{CH} = 0.45$, $t_O = 0.5$ and $d = \frac{1}{2}\sigma$. What makes the method robust is the fact that these values are not very critical and can be changed over a wide range without affecting the performance significantly.

The optimal value for the other two parameters, σ and f, are determined by their effect on the obtained curvature when applying the algorithm to synthetic data. Some smoothing is required to locate edges in the noisy data as used here, but this limits the curvatures that can be resolved. The results from the synthetic data show that curvatures up to $\frac{1}{2\sigma}$ can be resolved with an error less than 10%. The continuous representation of the pixelated edge can be done by a smoothing spline. Allowing for at least 1 px deviation ($f = 1$) is than required to suppress the noise in the resolved curvature, but a larger value is not advised since it introduces an offset in the mean curvature. This results in a method were solely one smoothing parameter, σ, needs to be set based on level of noise and the, to be expected, curvatures.

The method of selecting the good LoG edges based on their overlap ratio is compared to a more conventional method based on the gradient of the LoG. Although for the latter method a slightly higher performance can be obtained, this only hold for a narrow window of the respective threshold value. Outside this window the performance is greatly reduced. The optimal value will shift when data with different quality and/or intensity will be used, making this method less robust than our proposed method.

When evaluating actual flame front curvatures it is observed that the statistics obtained by the proposed method correspond very well with the statistics obtained by manually selecting the good LoG edges. There is an excellent agreement between the PDF's of the curvatures. So although there is some contamination of spurious edges (about 1%), the method is able to accurately measure the, for combustion relevant, flame front curvatures statistics, without the need for user intervention and for low quality data.

REFERENCES

1. J. Canny. A computational approach to edge detection. *Pattern Analysis and Machine Intelligence, IEEE Transactions on*, PAMI-8(6):679–698, 1986.
2. R. K. Cheng, D. Yegian, M. Miyasato, G. Samuelsen, C. Benson, R. Pellizzari, and P. Loftus. Scaling and development of low-swirl burners for low-emission furnaces and boilers. *Proceedings of the Combustion Institute*, 28(1): 1305–1313, 2000.
3. M. Day, S. Tachibana, J. Bell, M. Lijewski, V. Beckner, and R. K. Cheng. A combined computational and experimental characterization of lean premixed turbulent low swirl laboratory flames: I. methane flames. *Combustion and Flame*, 159(1):275 – 290, 2012.
4. K. Döbbeling, J. Hellat, and H. Koch. 25 years of bbc/abb/alstom lean premix combustion technologies. *Journal of Engineering for Gas Turbines and Power*, 129(1): 2–12, January 2007.
5. A. C. Eckbreth. *Laser Diagnostics for Combustion Temperature and Species*, volume 3 of *Combustion Science and Technology Book Series*. Gordon and Breach Publishers, Amsterdam, The Netherlands, 2nd edition, 1996.
6. M. Z. Haq, C. G. W. Sheppard, R. Woolley, D. A. Greenhalgh, and R. D. Lockett. Wrinkling and curvature of laminar and turbulent premixed flames. *Combustion and Flame*, 131(1-2): 1–15, 2002.
7. D. Marr and E. Hildreth. Theory of edge detection. *Proceedings of the Royal Society of London. Series B, Biological Sciences*, 207(1167):187–217, 1980.
8. N. Otsu. A threshold selection method from gray-level histograms. *IEEE Trans Syst Man Cybern*, SMC-9(1):62–66, 1979.
9. N. Peters. *Turbulent Combustion*. Cambridge University Press, 2004.
10. D. Price, R. Birnbaum, R. Batiuk, M. McCullough, and R. Smith. Nitrogen oxides: Impact on public health and the environment. Technical Report EPA-452/R-97/002, U.S. Environmental Protection Agency, Office of Air and Radiation, Washington, DC, 1997.
11. C. H. Reinsch. Smoothing by spline functions. *Numerische Mathematik*, 10:177–183, 1967.
12. A. Soika, F. Dinkelacker, and A. Leipertz. Pressure influence on the flame front curvature of turbulent premixed flames: comparison between experiment and theory. *Combustion and Flame*, 132(3):451–462, 2003.
13. M. S. Sweeney and S. Hochgreb. Autonomous extraction of optimal flame fronts in oh planar laser-induced fluorescence images. *Appl. Opt.*, 48(19):3866–3877, 2009.
14. M. S. Sweeney, S. Hochgreb, and R. S. Barlow. The structure of premixed and stratified low turbulence flames. *Combustion and Flame*, 158(5):935 – 948, 2011.
15. C. M. Vagelopoulos and J. H. Frank. Transient response of premixed methane flames. *Combustion and Flame*, 146(3): 572–588, 2006.
16. A. A. Verbeek, R. C. Pos, G. G. M. Stoffels, B. J. Geurts, and T. H. van der Meer. The generation of resonant turbulence for a premixed burner. In *ETMM9*, Thessaloniki, 2012.
17. Y. Yitzhaky and E. Peli. A method for objective edge detection evaluation and detector parameter selection. *IEEE Transactions on Pattern Analysis and Machine Intelligence*, 25(8):1027 – 1033, 2003.
18. F. T. C. Yuen and Ö. L. Gülder. Premixed turbulent flame front structure investigation by rayleigh scattering in the thin reaction zone regime. *Proceedings of the Combustion Institute*, 32(2):1747 – 1754, 2009.